THE JOURNAL OF COMPARATIVE NEUROLOGY 386:217–228 (1997)

Tangential Distribution of Cytochrome Oxidase-Rich Blobs in the Primary Visual Cortex of Macaque Monkeys

M.F. FARIAS,[1] R. GATTASS,[1]* M.C. PIÑÓN,[1] AND L.G. UNGERLEIDER[2]
[1]Departamento de Neurobiologia, Instituto de Biofísica Carlos Chagas Filho, Universidade Federal do Rio de Janeiro, Rio de Janeiro 21941-900, Brazil
[2]Laboratory of Brain and Cognition, National Institute of Mental Health, National Institutes of Health; Bethesda, Maryland 20892

ABSTRACT

We studied the tangential distribution of cytochrome c oxidase (CytOx)-rich blobs in four striate cortices of three normal monkeys (*Macaca mulatta*). The spatial density and cross-sectional area of blobs were analyzed in CytOx-reacted tangential sections of flat-mounted preparations of the striate cortex (V1). Well-delimited CytOx-rich blobs were found in the middle portion of cortical layer III of the V1. Throughout the binocular field representation, the spatial density of blobs was nearly constant with a mean value of four to five blobs per mm^2. In the monocular portions of V1, however, blob spatial density diminished. In all cases, the mean cross-sectional area of blobs was constant in the V1. The small variation of CytOx blob topography with visual field eccentricity contrasts with the variation described in previously published material. J. Comp. Neurol. 386:217–228, 1997.

Indexing terms: striate cortex; V1; modular organization; *Macaca mulatta*

The notion of cortical modules as repetitive subunits that analyze visual attributes of the image in small portions of the visual field was derived from single-unit studies by Hubel and Wiesel in the striate cortex (V1) of monkeys (for a review, see Hubel and Wiesel, 1977). These authors showed that the size of the cortical region in the V1 that represents a given point of the visual field is approximately 2 mm in diameter within the portion of the V1 representing the central 20° of the visual field. The linear dimension of the cortical "point image" (McIllwain, 1976) decreases toward the peripheral V1 (Dow et al., 1981) but is always large enough to contain neurons selective to all orientations and with dominance for each eye. This modular theory, as the basis for the processing of visual information in the cortex, was supported by the discovery of a periodic arrangement of functionally distinct subregions in the primate V1, as revealed by cytochrome oxidase (CytOx) histochemistry (Horton and Hubel, 1981; Livingstone and Hubel, 1982; Wong-Riley and Carroll, 1984; Carroll and Wong-Riley, 1984). These subregions have been given different names, such as "patches" (Horton and Hubel, 1981) "blobs" (Livingstone and Hubel, 1982), "spots" (Tootell et al., 1983), "puffs" (Carroll and Wong-Riley, 1984), or "dots" (Tigges et al., 1984; Hendrickson, 1985). In this paper we have used the name "blobs" to indicate the supragranular blobs because our analysis was restricted to layers II and III. The CytOx-rich "blobs" maintain invariant topographic relationships with ocular dominance (Horton and Hubel, 1981) and orientation columns (Blasdel and Salama, 1986).

Horton (1984) and Livingstone and Hubel (1984) reported that the size of the blobs in *Macaca mulatta* decreases with eccentricity, whereas the number of blobs per square millimeter increases. Thus, one could advocate that the cross-sectional area of blobs parallels the decrease of cortical "point image." In principle, therefore, CytOx blobs could be used as anatomical markers of a cortical modular organization. One study that questioned this idea, however, was that of Rosa et al. (1988), which found that the width of a pair of ocular dominance stripes in the New World monkey *Cebus* varied only slightly with eccentricity, for most of the V1. Because CytOx blobs occupy a central position relative to these stripes (Hess and Edwards, 1987), this observation suggested that the topographic distribution of blobs is invariant in the V1 in *Cebus*. In this respect, the *Cebus* was shown to be different

Grant sponsor: CEPG; Grant sponsor: CNP; Grant sponsor: FINEP.

Correspondence to: Dr. Ricardo Gattass, Departamento de Neurobiologia, Instituto de Biofisica Carlos Chagas Filho, Bloco G, CCS, Ilha do Fundão, Rio de Janeiro, RJ, 21941 Brazil.
E-mail: rgattass@chagas. biof.urfj.br

Received 13 August 1996; Revised 26 February 1997; Accepted 25 April 1997

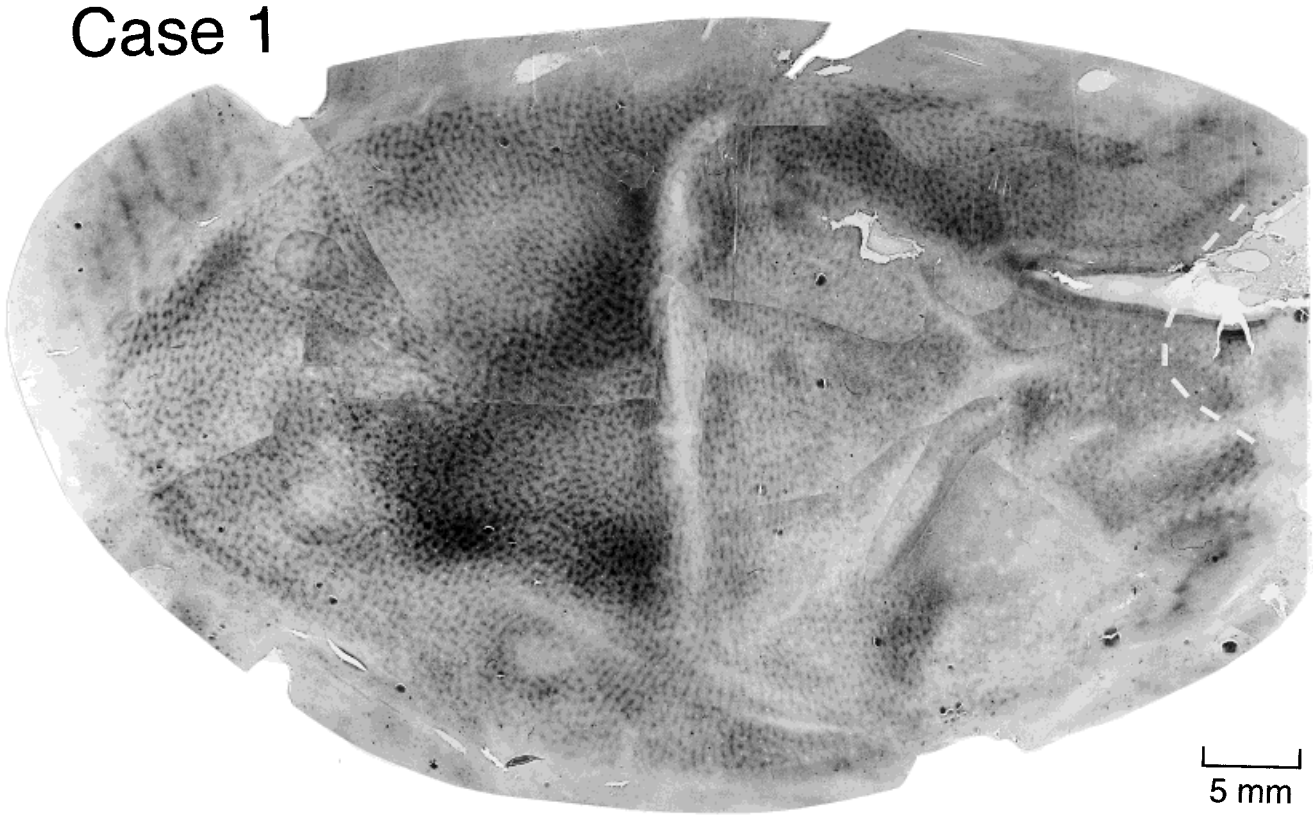

Fig. 1. Photographic montage showing the pattern of cytochrome oxidase (CytOx)-rich blobs in upper layers of the primary visual cortex (V1) in Case 1. Foveal V1 is at the left. The representation of the lower visual quadrant is at the top and that of the upper quadrant is at the bottom. The estimated border of monocular crescent is in white dashed line.

from *Macaca* because, in the latter species, the number of blobs per square millimeter was found to increase with increasing eccentricity (Horton, 1984; Livingstone and Hubel, 1984; Rosa et al., 1991). The discrepancy between *Macaca* and *Cebus* is surprising because the visual topography of the V1 and V2, the magnification factors, the orientation of ocular dominance stripes in the V1, and the cortical streams of visual information processing are similar in these genera (Gattass et al., 1981; Gattass et al., 1987; Gattass et al., 1990b; Rosa et al., 1988). The differences between *Cebus* and *Macaca* led us to reinvestigate the distribution of CytOx-rich blobs in the V1 of macaque monkeys. In this study, unlike previous ones, we used flattened preparations of the V1 to provide a direct comparison of blob size and density to the results described in *Cebus*. A preliminary account of these data has been published elsewhere (Gattass et al., 1995).

MATERIALS AND METHODS

Four cerebral hemispheres from three adult male *Macaca mulatta* monkeys were used. Ophthalmoscopic inspection of the eyes ensured that all animals were free from gross retinal abnormalities. A quantitative analysis of the CytOx blobs was performed in sections nearly tangential to cortical layer III from flattened preparations of striate cortex.

The monkeys were anesthetized with ketamine HCl (30 mg/kg) followed by a lethal dose of sodium pentobarbital. Following the occurrence of pharmacological apnea, the monkeys were perfused through the heart with a cold solution of 5% glycerol in phosphate buffer (0.1 M, pH 7.4). All of these procedures conform to NIH guidelines. Subsequently, the posterior portion of the brains underwent the flat-mounting procedure described by Tootell and Silverman (1985, Method II). The flat-mounted blocks were fixed between parafilm-covered glass slides in a 2.5% glutaraldehyde/20% glycerol in phosphate buffer solution for 24 hours. After fixation the blocks were embedded in albumin, quickly frozen, and cut at 40-μm sections on a freezing microtome. The sections were immediately mounted onto gelatinized slides, dried on a hot plate, and stored overnight in phosphate buffer. The cytochrome c oxidase histochemical reaction was performed by using the procedure modified by Silverman and Tootell (1987) from the protocol of Wong-Riley (1979). Stained sections were dehydrated, defatted, and coverslipped.

The sections were photographed by using Kodak Plus-X film under blue light illumination to increase contrast. Reconstruction of the pattern of CytOx blobs was accomplished by superimposing photographs of serial sections using blood vessels as landmarks (Rosa et al., 1988). For the quantitative analysis, blobs were outlined with fine-point permanent marker on enlarged (10×) contrast-

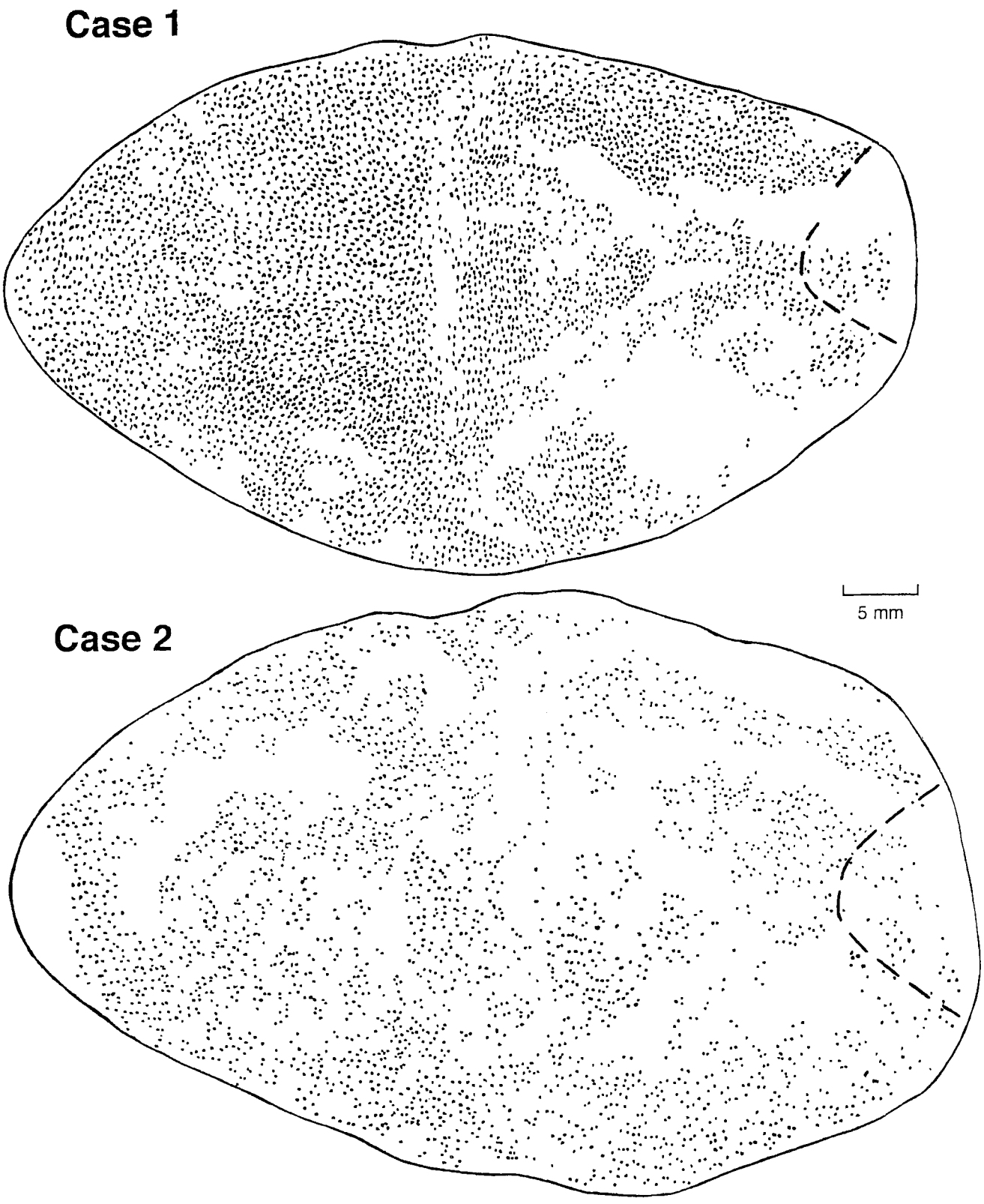

Fig. 2. Flattened reconstructions showing the drawings of CytOx-rich blobs in upper layers of the V1 of two monkeys. Orientation of the maps and conventions as in Figure 1.

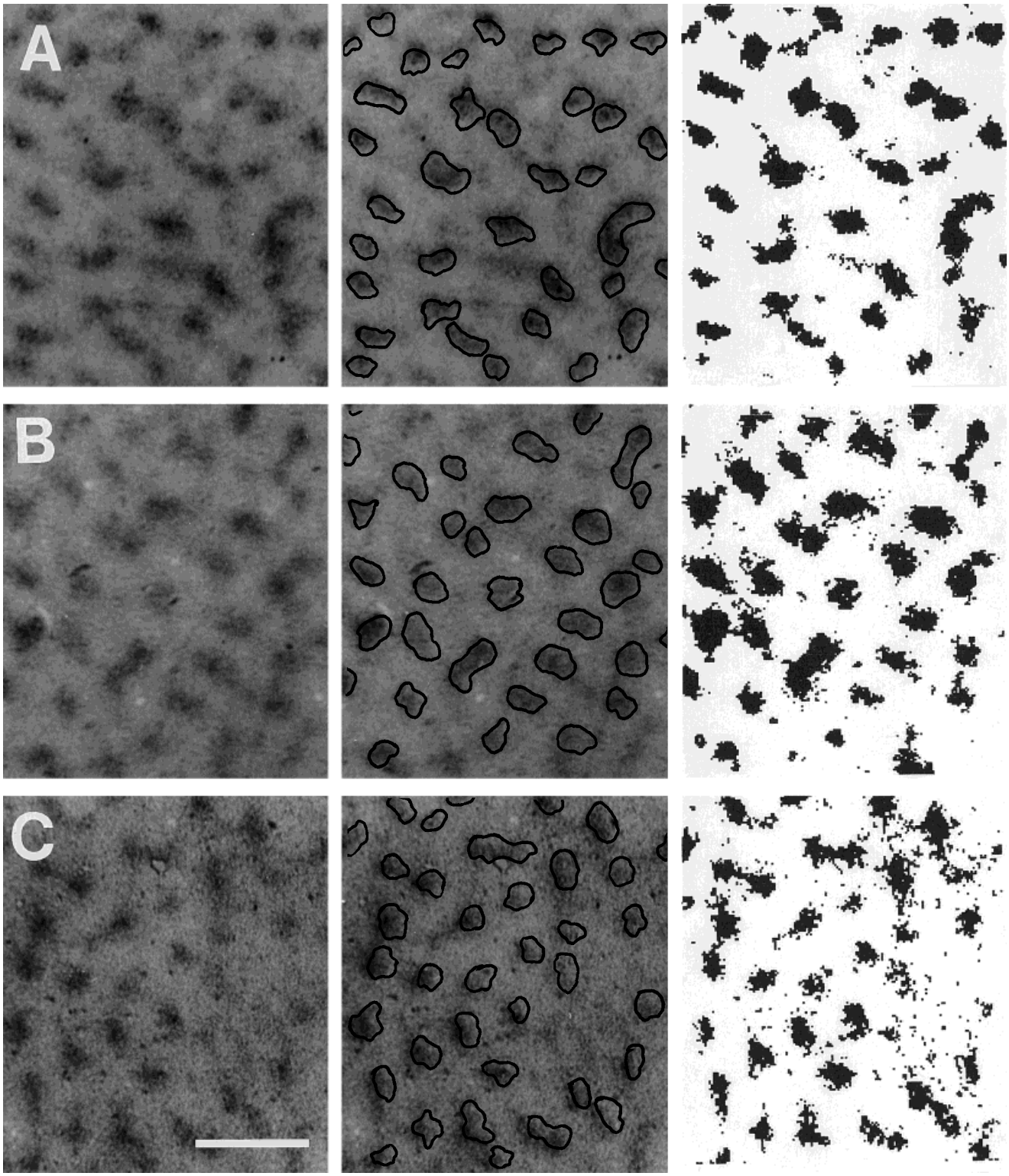

Fig. 3. Criteria used to draw cytox blob borders. Left: Photographs of cytox blobs in the V1 of Case 1; middle: same region with blobs outlined; right: computer-generated optical scans of the same regions subjected to the image processing techniques. The background was subtracted, and the contrast thresholds were set to 13% (**A**), 12% (**B**), and 14% (**C**). Row A correspond to 1.5°, row B to 3.75°, and row C to 30° eccentricity. Scale bar = 1 mm.

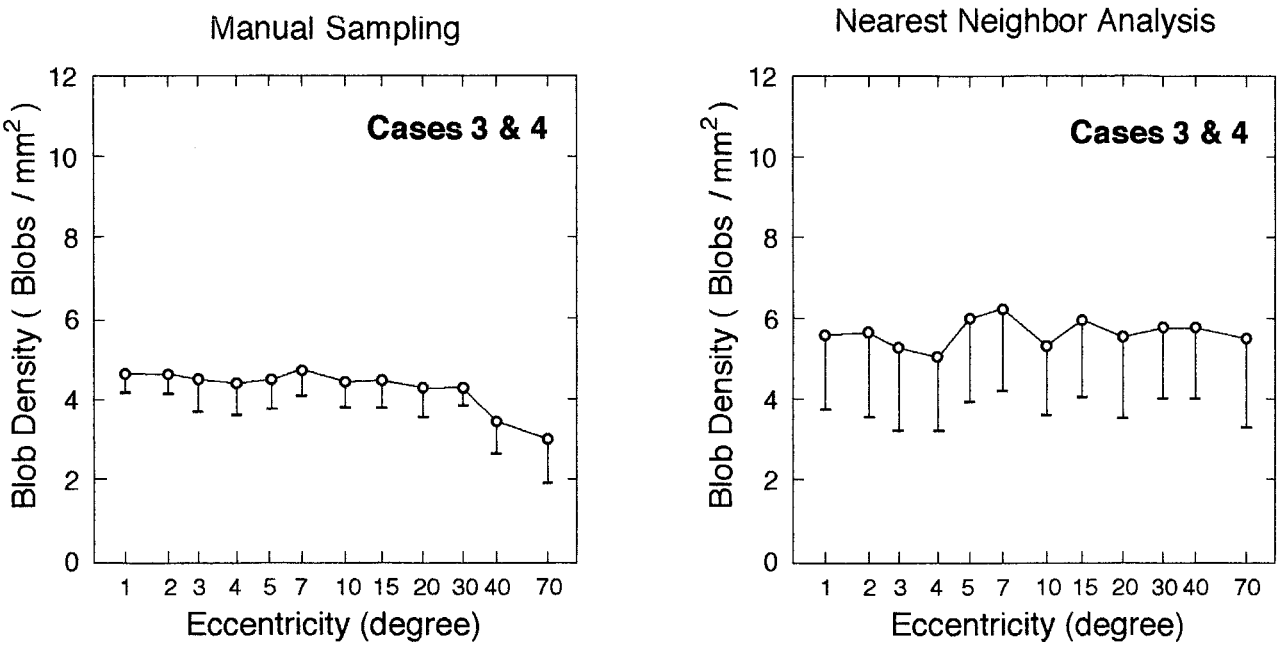

Fig. 4. Blob spatial density as a function of eccentricity in Cases 3 and 4 based on manual sampling (left) and nearest neighbor (right) analysis. Mean (circles) and standard deviation (bars) are along isoeccentric sectors.

matched prints of each section. The outlined blobs were then scanned and measured with the aid of a computer program (Image, courtesy of NIH) on an Apple Macintosh IIsi computer interfaced to a 600 dpi scanner. This program also provided the X-Y coordinates of the center of the blobs (centroids) used to calculate spatial density of the blobs. The density was determined by two methods. First, the number of blobs in a test square of 4 mm^2 were counted in every region of the V1 where all blobs were visible. Second, the mean density was calculated by using nearest neighbor analysis of blob centroids (Cases 3 and 4).

Because the location of the border of a given blob may vary depending on the cortical layer analyzed (Horton and Hubel, 1981; Livingstone and Hubel, 1984; Rosa et al., 1991), we analyzed blob topography at the middle portion of layer III, which shows the highest contrast between CytOx-rich (supragranular blobs) and CytOx-poor tissue. We tested for interobserver reliability by comparing measurements of the same hemisphere made by three different observers and found no statistically significant difference ($P > 0.3$). Nevertheless, for any given case, the measurements presented here are the average of the measurements of blobs drawn by at least two observers. In addition, we used an automated method for measurement of blob size and density because the manual method of outlining the blobs depends to a greater degree on subjective judgment. For the automated analysis, the photographic montages were scanned as gray tone-8 bit images, by using a 600 dpi scanner. The background of the original image was then subtracted by using a two-dimensional rolling ball (radius = 20) algorithm. A high-contrast black and white transformation was then made onto the filtered image using a threshold of 12–18%. The high-contrast representation of the blobs were then measured by using the same program used for the manual method, described above. In each hemisphere some cortical regions were not analyzed due either to tissue damage during the flattening procedure or to histological artifacts (Figs. 1 and 2). The assignment of retinotopic coordinates to specific sites in the flat-mounted V1 was made on the basis of the studies of Van Essen et al. (1984) and Gattass et al. (1981). The sizes of the V1 (in degrees) in different cases were normalized by multiplying the values of the magnification factors by constants to match the measured extent of the horizontal meridian representation (see Figs. 4, 5, 7, and 9).

In Results, data are shown for individual cases and for the group. Data from individual cases are shown as a function of eccentricity in degrees and in millimeters (see Figs. 5 and 9). Averaged data from the group of animals are shown as a function of eccentricity in degrees (see Figs. 4 and 7). In Discussion, data from different species are shown as a function of eccentricity in logarithmic scale (see Fig. 10).

RESULTS

The quantitative analysis presented here focuses on the size and distribution of CytOx-rich blobs within the middle third of layer III throughout the V1, where they are best delineated. In Figure 1 portions of adjacent sections through layer III of the V1 were combined to reconstruct the pattern of blobs for Case 1. As described previously (Horton, 1984; T'so and Gilbert, 1988), the shape of CytOx blobs in *Macaca* is irregular and tends to be oval. In some regions, adjacent blobs are linked by bridges of CytOx-reactive tissue, forming rows. In general, the highest contrast between blob and nonblob tissue is observed at the foveal representation (Fig. 1). At more peripheral locations, blob borders are fuzzy. Furthermore, bridges linking adjacent blobs are also more frequent at the foveal representation (Fig. 1). Flattened reconstructions of the V1 showing the distribution of the blobs in Cases 1 and 2

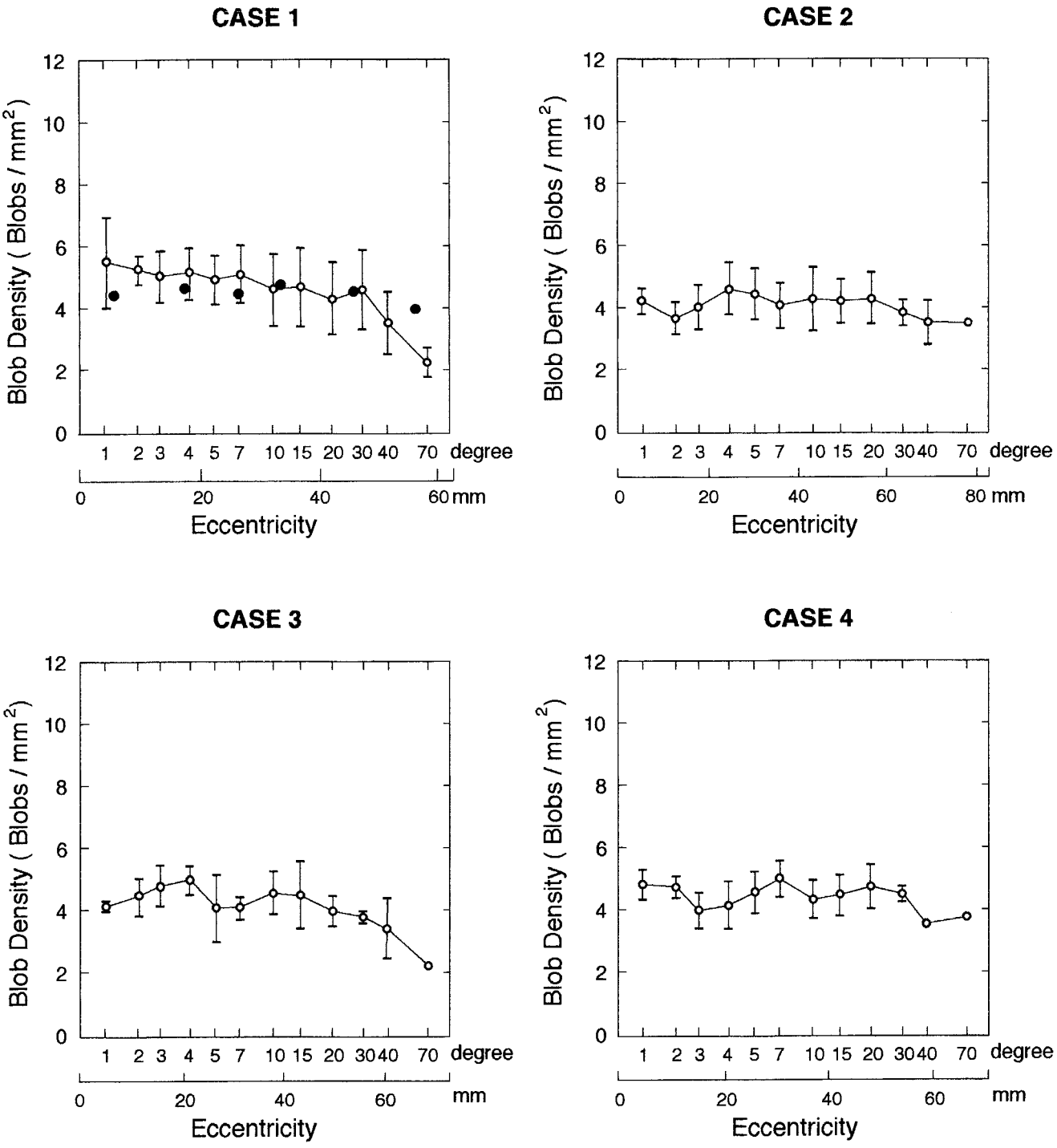

Fig. 5. Blob spatial density as a function of eccentricity, in degrees and in millimeters, in four cases. Mean (circles) and standard deviation (bars) of direct measurements (manual sampling) along isoeccentric sectors. Standard deviation smaller than the mean symbols at the peripheral region in the V1 reflect the small size of the samples. Data from automated analyses are shown by filled circles.

are shown in Figure 2. As shown in this figure, the shapes of the blobs in Case 1 are similar to those in Case 2.

Automated analysis vs. manual analysis

Figure 3 illustrates three different sectors of the area V1 representing 1.5 (A), 3.75 (B), and 30° (C) eccentricity, respectively, and shows manual delimitation of blobs and automated high-contrast blobs. Subsequent analyses (Case 1 in Figs. 5 and 9) revealed a similar blob cross-sectional area and blob density with both methods. We opted for the manual method because the automated analysis required arbitrary thresholds and arbitrary size filters to be se-

lected (Purves and LaMantia, 1993). In addition, in some cases, some blobs did not have sufficient contrast to be counted automatically or were attached to an adjacent blob and, therefore, by not being counted separately, generating errors. In Figure 3B some blobs corresponding to 3.75° eccentricity did attach to their adjacent neighbors by using the automated method. As a result, the mean blob area and the standard deviation were bigger than the ones obtained by the manual method (Fig. 9, Case 1, arrowhead). Blob density corresponding to that eccentricity (Fig. 5) decreased for the same reason.

Blob spatial density

Blob density, the number of blobs per mm^2, was obtained by direct measures (manual sampling) in all cases (3–5 blobs/mm^2) and by calculating the mean spatial density, using nearest neighbor analysis in Cases 3 and 4 (5–6 blobs/mm^2). Blob density varied from 1.8 to 8.0 blobs/mm^2 with a median of 4.5 blobs/mm^2 (Fig. 8, bottom). A reduction in blob spatial density at the monocular crescent in the V1 was observed only by using the manual sampling method (Fig. 4). The decrease in blob density at the monocular crescent did not appear in the analysis of blob density based on the nearest neighbor analysis. Although this decline was visible at the monocular crescent, the mean distance between blobs did not vary. We interpret this apparent discrepancy as a tendency for blobs to be maintained in rows, despite the absence of rows corresponding to the ipsilateral eye in the monocular crescent. Thus, although the blobs corresponding to the contralateral eye keep their nearest neighbor distances at the same range as that of the binocular field representation, each blob in a row is more separated from others in neighboring rows. For these reasons, we decided to use the direct measurement method in all cases to show the variation of density with eccentricity. The absolute value of blob density in the binocular region is, however, better evaluated by the nearest neighbor method (5–6 blobs/mm^2).

Figure 5 shows the variation of blob spatial density with eccentricity in the four cases. This figure illustrates that, in the four hemispheres of normal macaques, blob spatial density is fairly constant throughout the binocular portion of the V1. Blob density in the V1 did not vary with polar angle (Fig. 6). In each case, the number of blobs/mm^2 showed small variation along the polar sectors considered. Averaging across animals (Fig. 7, bottom), there was no significant variation in blob spatial density with eccentricity in the binocular representation of the visual field. The number of blobs/mm^2 at different eccentricities in Cases 1 and 3 showed a decrease in blob density in the monocular crescent. In these cases, a significantly smaller blob density was observed at the monocular periphery compared with neighboring portions of the binocular field ($P < 0.05$).

The small size of the monocular crescent (approximately 6×12 mm) and the distortions introduced at the very end of the calcarine fissure by the flattening procedure contribute to a smaller sample (68 blobs) in this region. In addition, the contrast of the blobs in the monocular crescent is low, which reduces the number of square probes (8) used to determine blob density. Thus, the decrease in blob density that was observed in two of four cases should be further evaluated with a bigger sample.

Blob spatial density varied among animals. Monkeys with large striate cortices tended to show smaller blob spatial density. Data presented in Table 1 suggest a linear correlation between the surface area of the V1 and blob density (Density = 6.722–0.002 * V1 size; $r = 0.88$).

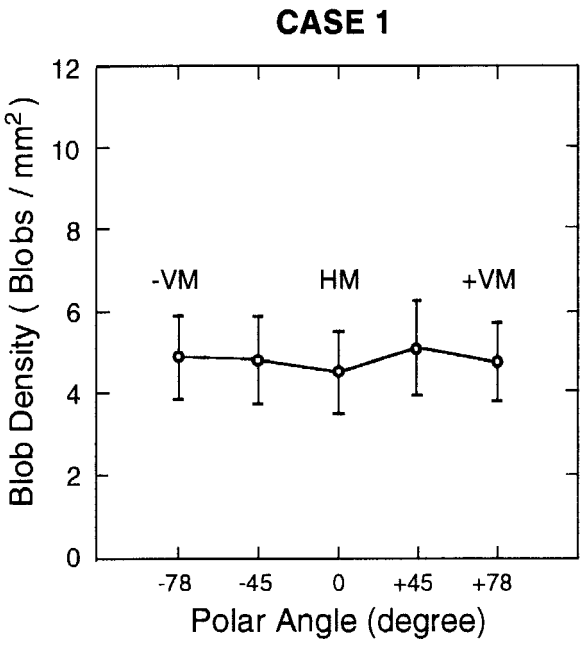

Fig. 6. Blob spatial density as a function of polar angle in Case 1. Mean and standard deviation of direct measurements (manual sampling) along isopolar sectors. Conventions as in Figure 5.

Blob cross-sectional area

The size of the blobs in the middle portion of layer III in the V1 ranged from 0.020 to 0.135 mm^2, with a median of 0.55 mm^2 (Fig. 8, top). Blob cross-sectional area did not vary consistently with eccentricity (Fig. 7, top). There was a small variability in the mean blob area among individual monkeys (Fig. 9). There was no correlation between mean blob area and the size of the V1 (Table 1). As in *Cebus* (Rosa et al., 1991), within the binocular field representation, the fraction of the V1 surface corresponding to CytOx-rich blob tissue tended to decrease toward the periphery. Blobs covered approximately 24% of the surface area of the V1.

DISCUSSION

Comparison with previous studies in *Macaca*

We found that CytOx-rich blobs tend to be largest in the middle portion of layer III, as previously reported by Trusk et al. (1990) in the *Macaca fascicularis*. As mentioned in Materials and Methods, the size of the blobs depends on the criteria used to draw their borders. In all cases and throughout the area, the same criteria were used. However, our conclusions on the distribution of size and density of Cytox blobs must be considered in light of several limitations of the present study, such as 1) the sample at the monocular crescent is small in three animals and 2) the flat-mounted procedure includes compression of a folded piece of an unfixed tissue that may stretch unevenly, contributing to local distortions in the area. In this study we focused on the variation of size and of density with eccentricity rather than on their absolute values.

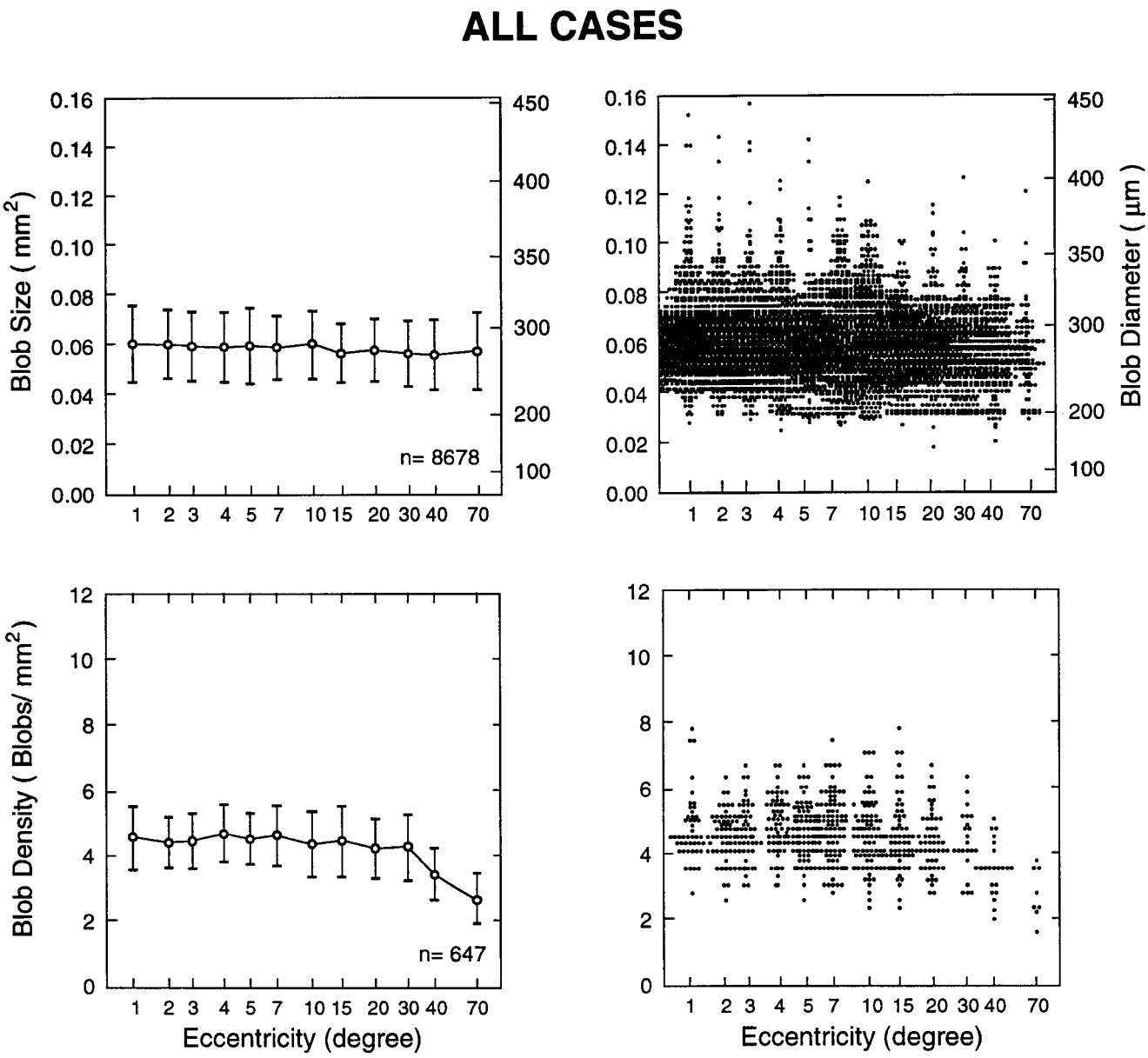

Fig. 7. Blob cross-sectional area (top) and blob density (bottom) as a function of eccentricity. Data from all cases. Mean and standard deviation (right) from measurements (left) along isoeccentric sectors. Conventions as in Figure 5.

TABLE 1. Mean Blob Density, Area, Diameter, and Surface Area of the V1 in Each Hemisphere

	Blob density (blobs/mm^2)	Blob area (mm^2)	Blob diameter (µm)	Area of V1 (mm^2)
Case 1	4.6	0.058	272	1,110
Case 2	3.6	0.057	269	1,473
Case 3	4.1	0.061	279	1,198
Case 4	4.1	0.062	281	1,128

Horton (1984) described an increase in blob density with increasing eccentricity within the representation of the binocular field in macaque. In one of the cases illustrated in his study (Horton, 1984, Fig. 12) blob density reached 9 blobs/mm^2 at the representation of far peripheral vision, at the border of the monocular field, whereas values at the occipital operculum, i.e., at the representation of central vision, were approximately 5 blobs/mm^2. An increase in blob density with increasing eccentricity in macaques was also reported by Livingstone and Hubel (1984) at the representation of the central 10° of the visual field. These authors reported a mean blob density of 3.45 blobs/mm^2 and a mean blob area value of 0.05 mm^2. These mean values are close to the ones we report in this study. However, we found that blob density remains nearly constant throughout the binocular field. These trends differ from previously published data in the macaque (Horton, 1984; Livingstone and Hubel, 1984) determined in small tangential segments of the opercular surface and

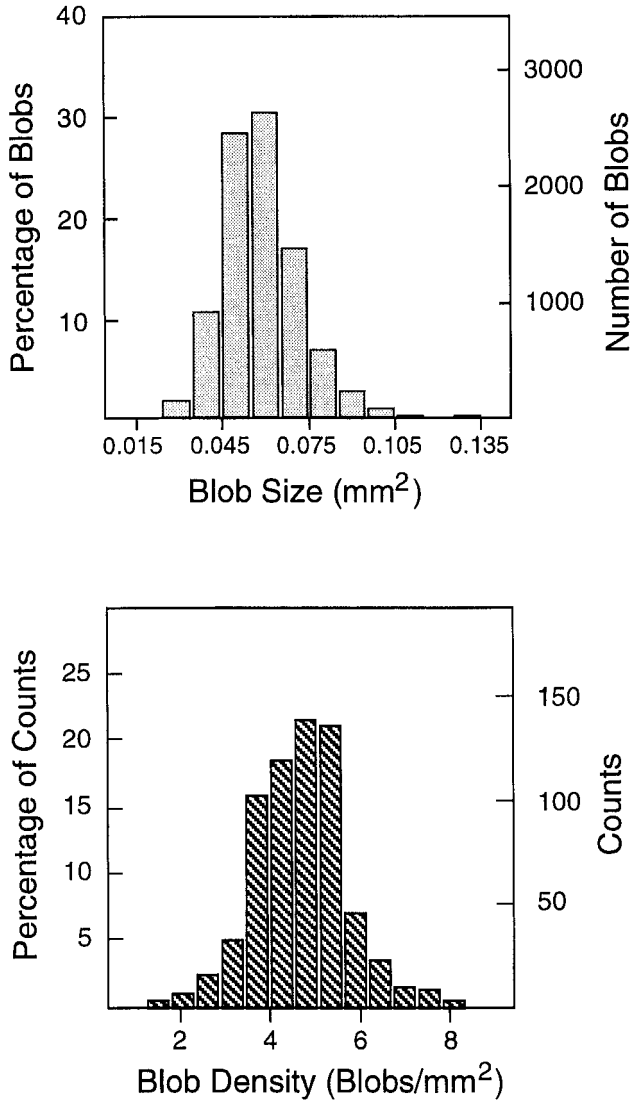

Fig. 8. Histograms of blob cross-sectional area (**top**) and blob density (**bottom**) from all cases.

roof of the calcarine fissure (Fig. 10). The difference in the variation of blob size and blob density with eccentricity is probably related to differences in the type of preparation used and to the limited extent of the analysis in previous studies (Wong-Riley, 1994). Another hypothesis that could account for these differences is related to a possible monocular foveal retinal lesion in the case studied by Livingstone and Hubel (1984). Foveal lesions in humans cause an increase in size and a decrease in density of the CytOx-rich blobs (Moura et al., 1994). Purves and LaMantia (1993) studied the development of blobs in the area V1 of *Macaca mullata* and reported that the number of blobs remains approximately the same between birth and maturity. In adult monkeys, they described a blob area of 0.025 mm^2 and a density of 4.3 blobs/mm^2 by using automated analysis and a blob area of 0.066 mm^2 and a density of 4.7 blobs/mm^2 by using camera lucida tracings.

In the present study, we found an abrupt decrease in blob spatial density at the transition from the binocular to the monocular representation in the V1 (Fig. 5), which is similar to that described by Horton (1984). The reported value for *Macaca fascicularis* (5.5 blobs/mm^2) is somewhat smaller than that of *Macaca mulatta* (6.0 blobs/mm^2). It is reasonable to conclude that this differential spatial distribution of blobs in the binocular vs. monocular field might be related to the absence of ocular dominance stripes within the monocular crescent.

Cytochrome oxidase blobs in other primates

The variation of blob spatial density with eccentricity determined in flattened preparations of the V1 of macaques is similar to those determined by using similar methods in *Cebus* (Rosa et al., 1991) and in *Homo* (Moura et al., 1994).

Cytochrome oxidase-rich blobs were previously investigated in the V1 of *Cebus* by Hess and Edwards (1987), who analyzed the occipital operculum of a single specimen. These authors reported a mean blob area value of 0.05 mm^2 and a mean blob density of 3.45 blobs/mm^2. These values are very close to the ones reported previously in large *Cebus* monkeys (Rosa et al., 1991), despite the different methods used in tissue processing and in the quantitative analysis. However, we observed in this study a considerable variability in blob density among the four cases. As in *Cebus*, we also observed in two cases that blobs tend to be individualized, with few obvious bridges of CytOx-reactive tissue between them. This tendency may be related to the less conspicuous arrangement in rows in some animals. The difference in the variation of blob cross-sectional area with eccentricity in macaque (present study) and *Cebus* (Rosa et al., 1991) may be due to interspecies differences (Fig. 10). The size of the blobs in *Macaca* are larger than those in *Cebus* (Rosa et al., 1991) and smaller than those in *Homo* (Moura et al., 1994). Therefore, we are confident that these differences between *Cebus*, *Homo*, and *Macaca* are real, because similar flattening procedures and similar morphometric analysis were used.

Among New World monkeys, there are interspecies differences relative to blob size, density, and regularity of distribution. In the squirrel monkey (*Saimiri*), Horton (1984) found that blobs were rounder, smaller, and more clearly separated than those of macaques. The data on blob density may also imply differences between New and Old World monkeys, because the macaque shows a high blob density, which is even higher than that of the marmoset, despite the macaque's large striate cortex. Moreover, data illustrated by Cusick and Kaas (1988, Fig. 2) and by Tootell et al. (1985) suggest that, in squirrel and owl monkeys, as in the *Cebus* (Rosa et al., 1991), blob density may not increase toward the peripheral representation.

The regular distribution of blobs in *Saimiri*, which follows a square or hexagonal grid, also contrasts with the pattern found in *Cebus* (Rosa et al., 1991). The clear separation of blobs and their regular distribution are characteristics of CytOx blob topography in the marmoset *Callithrix jaccus* (Gattass et al., 1990a), suggesting that this may be a general pattern of small New World monkeys, which lack ocular dominance columns (Rosa et al., 1988). With regard to blob density, the estimates of Rosa et al. (1991) in *Cebus* (4.0 blobs/mm^2), Horton (1984) in *Saimiri* (4.5 blobs/mm^2), and Gattass et al. (1990a) in *Callithrix* (approximately 6.0 blobs/mm^2) suggest that blobs are compressed in these smaller species. Note, however, that the surface of striate cortex in the marmoset

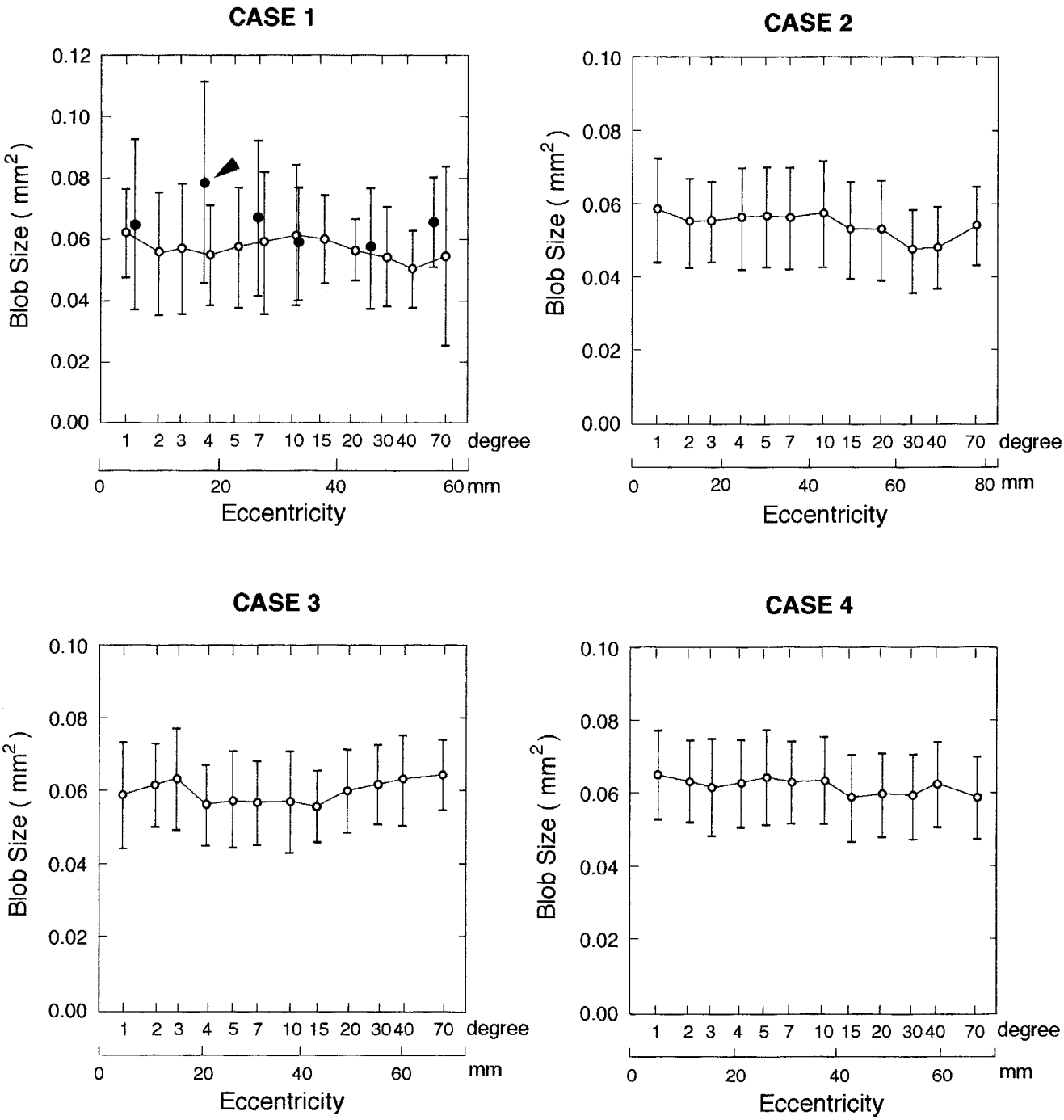

Fig. 9. Blob cross-sectional area as a function of eccentricity in degrees and in millimeters in four cases. Conventions as in Figure 5. Confluent blobs in the automated analysis led to discrepant mean value (arrowhead) and large standard deviation (see text).

is approximately one-fifth of that in *Cebus*, whereas blob topography is not proportionally compressed. This result leads one to conclude that the organization of striate cortex in small monkeys is not a simple compression of that found in the large ones.

The nocturnal owl monkey, *Aotus*, shows a relatively low blob density with respect to the size of the V1 (2.5 blobs/mm^2, Tootell et al., 1985). CytOx blobs in this animal also differ from those in other primates because they are visible in all cortical layers, including layer IVc. These differences may be related to the nocturnal/crepuscular habits of this unique simian (Wright, 1981).

In *Homo*, Horton and Hedley-White (1984) reported a blob density of 1.25–1.67 blobs/mm^2, whereas Wong-Riley et al. (1993) reported a value of 2–3 blobs/mm^2. More recently, Moura et al. (1994) studied a much larger sample

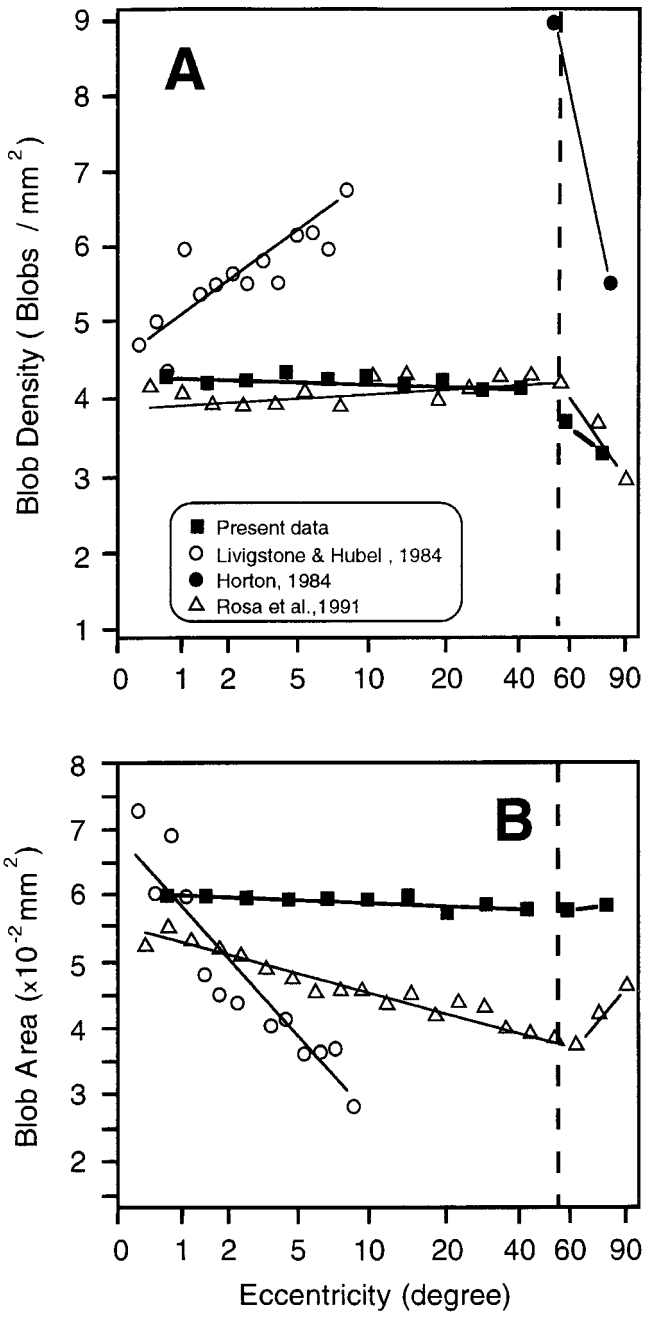

Fig. 10. Comparison of blob density (**A**) and blob cross-sectional area (**B**) in *Cebus apella*, *Macaca mulatta*, and *Macaca fascicularis*. In all cases, straight lines were fitted to the data along the presumptive binocular field representation to express the mean variation of the data with eccentricity. The approximate eccentricity of the inner limit of the monocular field is shown as a dotted line.

and reported a blob density of 1.2 blobs/mm^2, a value similar to the one reported by Horton and Hedley-White (1984).

Cytochrome oxidase blobs and cortical modules in the V1

In the V1 of *Macaca*, CytOx blobs are coextensive and in register with ocular dominance stripes (Horton and Hubel, 1981; Hess and Edwards, 1987). Therefore, the smallest conceivable cortical module would encompass a minimum of two CytOx blobs, one for each eye. However, not all blobs are alike. T'so and Gilbert (1988) studied the central visual field representation in the V1 of macaques and showed that CytOx blobs are usually of two different types, i.e., the blobs that encompass neurons selective to red/green (RG) color contrast and those containing blue/yellow (BY)-selective neurons. These types of blobs occur in a 3:1 ratio, respectively, in the central V1. In addition, a third type of CytOx blob may exist, containing neurons responsive to broadband (BB) stimuli. Therefore, as previously pointed out by Rosa et al. (1991), a cortical point image in the central V1 of macaques must contain all the neuronal machinery for the analysis of a given point of the visual field. This area, that encompasses at least 8, and possibly 10 or more CytOx blobs (3 RG: 1 BY: 1 BB blobs $\times$ 2 eyes), occupies approximately 2 mm^2 and is in close agreement with the estimates of the central point image area. In this model, point images in the V1 would vary as a function of the relative numbers of RG, BY, and BB blobs at different eccentricities. At the monocular representation one might predict the existence of a different type of module with blobs related only to the contralateral eye and BB stimuli. In this region, blobs are described to be larger, rounder, and more widely spaced than in the binocular region and the density is believed to decrease to half (Horton, 1984). The present study confirms this decrease in blob density in the monocular crescent, although this decrease was found to be less pronounced than that described by Horton (1984).

ACKNOWLEDGMENTS

We thank J.N. Sewell III for help in histology and E. Saturato da Silva Filho for photography.

LITERATURE CITED

Blasdel, G.G., and G. Salama (1986) Voltage-sensitive dyes reveal a modular organization in monkey striate cortex. Nature *321:*579–585.

Carroll, E.W., and M.T.T. Wong-Riley (1984) Quantitative light and electron microscopic analysis of cytochrome oxidase-rich zones in the striate cortex of the squirrel monkey. J. Comp. Neurol. *222:*1–17.

Cusick, C.G., and J.H. Kaas (1988) Cortical connections of area 18 and dorsolateral visual cortex in squirrel monkeys. Visual Neurosci. *1:*211–237.

Dow, B.M., A.Z. Snyder, R.G. Vautin, and R. Bauer (1981) Magnification factor and receptive field size in foveal striate cortex of the monkey. Exp. Brain Res. *44:*213–228.

Gattass, R., C.G. Gross, and J.H. Sandel (1981) Visual topography of V2 in the macaque. J. Comp. Neurol. *201:*519–539.

Gattass, R., A.P.B. Souza, and M.G.P. Rosa (1987) Visual topography of V1 in the *Cebus* monkey. J. Comp. Neurol. *259:*529–548.

Gattass, R., M.G.P. Rosa, A.P.B. Sousa, M.C.G.P. Piñón, M. Fiorani, Jr., S. Neuenschwander, M.M. Moura, J.H. Abrahäo, and P.E.S. Saraiva (1990a) Visual topography and modular organization of cortical areas in primates. In E. Iwai and M. Mishkin (eds): Vision, Memory and Temporal Lobe. New York: Elsevier, pp. 355–367.

Gattass, R., M.G.P. Rosa, A.P.B. Sousa, M.C.G.P. Piñón, M. Fiorani, Jr., and S. Neuenschwander (1990b) Cortical streams of visual information processing in primates. Braz. J. Med. Biol. Res. *23:*375–393.

Gattass, R., M.F. Farias, M.C. Piñón, and L.G. Ungerleider (1995) Distribution of cytocrome oxidase-rich patches in the primary visual cortex of macaque monkeys. Soc. Neurosci. Abstr. *21:*904.

Hendrickson, A.E. (1985) Dots, stripes and columns in monkey visual cortex. Trends Neurosci. *8:*406–410.

Hess, D.T., and M.A. Edwards (1987) Anatomical demonstration of ocular segregation in the retinogeniculocortical pathway of the New World capuchin monkey (*Cebus apella*). J. Comp. Neurol. *264:*409–420.

Horton, J.C. (1984) Cytochrome oxidase patches: A new cytoarchitectonic feature of monkey visual cortex. Philos. Trans. R. Soc. London B *304:*199–253.

Horton, J.C., and E.T. Hedley-Whyte (1984) Mapping of cytochrome oxidase patches and ocular dominance columns in human visual cortex. Philos. Trans. R. Soc. Lond. B *304:*255–272.

Horton, J.C., and D.G. Hubel (1981) Regular patchy distribution of cytochrome oxidase staining in primary visual cortex of macaque monkey. Nature *292:*762–764.

Hubel, D.H., and T.N. Wiesel (1977) Functional architecture of macaque monkey visual cortex: Ferrier lecture. Proc. R. Soc. Lond. [Biol] *198:*1–59.

Livingstone, M.S., and D.H. Hubel (1982) Thalamic inputs to cytochrome oxidase-rich regions in monkey visual cortex. Proc. Natl. Acad. Sci. USA *79:*6098–6101.

Livingstone, M.S., and D.H. Hubel (1984) Anatomy and physiology of a color system in the primate visual cortex. J. Neurosci. *4:*309–356.

McIllwain, J.L. (1976) Large receptive fields and spatial transformations in the visual system. Int. Rev. Physiol. *10:*223–249.

Moura, M.M., R. Gattass, L.F. Pary, and M.F. Farias (1994) Changes in cytocrome oxidase-rich patches in striate cortex of humans with retinal lesions. Soc. Neurosci. Abstr. *20:*1110.

Purves, D., and A. LaMantia (1993) Development of blobs in the visual cortex of macaques. J. Comp. Neurol. *334:*169–175.

Rosa, M.G.P., R. Gattass, and M. Fiorani, Jr. (1988) Complete pattern of ocular dominance stripes in V1 of a New World monkey, *Cebus apella*. Exp. Brain Res. *72:*645–648.

Rosa, M.G.P., R. Gattass, and J.G.M. Soares (1991) A quantitative analysis of cytochrome oxidase-rich patches in the primary visual cortex of *Cebus* monkeys: Topographic distribution and effects of late monocular enucleation. Exp. Brain Res. *84:*195–209.

Silverman, M.S., and R.B.H. Tootell (1987) Modified technique for cytochrome oxidase histochemistry: Increased staining intensity and compatibility with the 2-deoxyglucose autoradiography. J. Neurosci. Methods *19:*1–10.

Tigges, M., A.E. Hendrickson, and J. Tigges (1984) Anatomical consequences of long-term monocular eyelid closure on lateral geniculate nucleus and striate cortex in squirrel monkey (*Saimiri*). J. Comp. Neurol. *148:*481–490.

Tootell, R.B.H., and M.S. Silverman (1985) Two methods for flat-mounting cortical tissue. J. Neurosci. Methods. *15:*177–190.

Tootell, R.B.H., M.S. Silverman, R.L. De Valois, and G.H. Jacobs (1983) Functional organization of the second cortical visual area in primates. Science *220:*737–739.

Tootell, R.B.H., S.L. Hamilton, and M.S. Silverman (1985) Topography of cytochrome oxidase activity in owl monkey cortex. J. Neurosci. *5:*2786–2800.

Trusk, T.C., W.S. Kaboord, and M.T.T. Wong-Riley (1990) Effects of monocular enucleation, tetrodotoxin, and lid suture on cytochromeoxidase reactivity in supragranular puffs of adult macaque striate cortex. Visual Neurosci. *4:*185–204.

T'so, D.Y., and C.D. Gilbert (1988) The organization of chromatic and spatial interactions in the primate striate cortex. J. Neurosci. *8:*1712–1727.

Van Essen, D.C., W.T. Newsome, and J.H.R. Maunsell (1984) The visual field representation in striate cortex of macaque monkey: Assymmetries, anisotropies and individual variability. Vision Res. *24:*429–448.

Wong-Riley, M.T.T. (1979) Changes in the visual system of monocularly sutured or enucleated kittens demonstrable with cytochrome oxidase histochemistry. Brain Res. *171:*11–28.

Wong-Riley, M.T.T. (1994) Primate visual cortex: Dynamic methabolic organization and plasticity revealed by cytochrome oxidase. Cereb. Cortex *10:*141–200.

Wong-Riley, M.T.T., and E.W. Carroll (1984) Quantitative light and electron microscopic analysis of cytochrome oxidase-rich zones in VII prestriate cortex of the squirrel monkey. J. Comp. Neurol. *222:*18–37.

Wong-Riley, M.T.T., R.F. Hevner, R. Cutlan, M. Earnest, R. Egan, J. Frost, and T. Nguyen (1993) Cytochorome oxidase in the human visual cortex: Distribution in the developing and the adult brain. Visual Neurosci. *10:*41–58.

Wright, P.C. (1981) The night monkeys, genus *Aotus*. In A.F. Coimbra Filho and R.A. Mittermeier (eds): Ecology and Behavior of Neotropical Primates. Rio de Janeiro: Academia Brasileira de Ciências.